Physics of the Earth and Planetary Interiors 323 (2022) 106824

Contents lists available at ScienceDirect

Physics of the Earth and Planetary Interiors

journal homepage: www.elsevier.com/locate/pepi

Thermal equation of state of F-bearing superhydrous phase B ($Mg_{10}Si_3O_{14}(OH,F)_4$): Implications for the transportation of fluorine and water into the lower mantle

Xiang Li [a,1], Yungui Liu [a,b], Ran Wang [c], Takashi Yoshino [c], Jingui Xu [d], Dongzhou Zhang [d], Tobias Grützner [e], Junfeng Zhang [a], Xiang Wu [a,*]

[a] State Key Laboratory of Geological Processes and Mineral Resources, China University of Geosciences (Wuhan), Wuhan 430074, China
[b] College of Gems and Materials, Hebei GEO University, Shijiazhuang 050031, China
[c] Institute for Planetary Materials, Okayama University, Misasa, Tottori 682-0193, Japan
[d] School of Ocean and Earth Science and Technology, Hawai'i Institute of Geophysics and Planetology, University of Hawai'i at Manoa, Honolulu 96822, HI, USA
[e] Institut de minéralogie, de physique des matériaux et de cosmochimie, Sorbonne Université, 4, Place Jussieu - BC 115, 75252 Paris Cedex 5, France

ARTICLE INFO

Keywords:
F-bearing Shy-B
Thermal equation of state
Elasticity
Water

ABSTRACT

Superhydrous phase B (Shy—B), an important hydrous magnesium silicate, plays a key role in the transportation of water from upper to lower mantle via subduction slabs. Moreover, it may also be a potential carrier for another important volatile element: fluorine (F). To explore the influence of F on mantle minerals and its behaviors during subducting, we investigated the compressibility of F-bearing Shy-B using synchrotron-based single-crystal X-ray diffraction combined with diamond anvil cells up to 27 GPa and 750 K. Our results show that the substitution of OH by F can enhance the incompressibility of Shy—B. Based on the obtained thermal elastic parameters, density and velocity profiles are evaluated along cold and warm slabs. Our results demonstrate that the addition of F enhances the bulk velocity (~1.0–2.4%) of Shy-B relative to the OH end-member at uppermost lower mantle conditions. The decomposition of F-bearing Shy-B into bridgmanite and periclase would lead to a small increase in bulk velocity (~0.7–1.8%). Thus, the accumulation and decomposition of F-bearing Shy-B is hard to explain the velocity anomaly at the uppermost lower mantle. Our results provide constraints for modeling the geodynamic process related to subduction and transportation of F and H_2O into the lower mantle.

1. Introduction

Volatiles have strong effects on the fractional crystallization of magmas, viscosity of melts, and rheology of mantle minerals. Therefore, it is essential to study the distribution and cycling mechanisms of volatile elements such as hydrogen (H), carbon (C) and halogen group (F, Cl, Br and I) in the Earth's mantle. The deep cycling of H has been extensively studied during last few decades. Previous studies show that major minerals (wadsleyite and ringwoodite) in the transition zone can incorporate up to 30,000 μg/g water. (e.g. Smyth, 1987; Inoue, 1994; Kohlstedt et al., 1996). While major minerals of the upper mantle (e.g. olivine, pyroxene) and the lower mantle (e.g. bridgmanite) accommodate significantly less water. Recently, the behaviors of F in the deep Earth has been studied seriously due to its similar ionic radius with $(OH)^-$. F concentrations in the Mid Ocean Ridge Basalt (MORB) and Oceanic Island Basalt (OIB) range from 16 to 109 μg/g (Schilling et al., 1980; Saal et al., 2002) and from 34 to 76 μg/g (Joachim et al., 2015) respectively, which are both higher than the estimate for bulk silicate Earth (BSE) (25 μg/g: McDonough and Sun, 1995). Therefore, the high abundance of F in the deep Earth might have been incorporated into the major mantle minerals.

The solubility of F in various mantle minerals has been determined in recent years. Natural olivine and pyroxene can incorporate up to 50 μg/g of F (e.g. Mosenfelder and Rossman, 2013a, 2013b). High-temperature and high-pressure experimental (HTHP) results show that a large amount of F can be stored in olivine (up to 5100 μg/g, Grützner et al., 2017a), pyroxenes (660 μg/g, Dalou et al., 2012), pyrope (1100 μg/g, Bernini et al., 2012), wadsleyite (1045 μg/g) and ringwoodite (1235 μg/

* Corresponding author.
E-mail address: wuxiang@cug.edu.cn (X. Wu).
[1] Now at Institut für Mineralogie, Universität Münster, Corrensstraße 24, D-48149 Münster, Germany.

https://doi.org/10.1016/j.pepi.2021.106824
Received 2 February 2021; Received in revised form 21 September 2021; Accepted 1 November 2021
Available online 3 November 2021

g) (Roberge et al., 2015; Grützner et al., 2018). Bridgmanite, the dominant mineral in the lower mantle, can also incorporate up to12917 μg/g of F (Yoshino and Jaseem, 2018). One source of F in the Earth's mantle is proposed to be transported from the Earth's surface into deep mantle by subduction slabs, like the cases of H and C. Although F is partially released during dehydration of oceanic crust and degassed through arc volcanism, ~95% of the subducted F is estimated to be transported into the deep mantle (Straub and Layne, 2003) with an annual global flux of about 9.9–10 × 10^{12} g (John et al., 2011). Most dominant mantle minerals are nominally F-free and do not contain more than a few thousand μg/g of F. However, a small component of F can significantly affect the properties of minerals, such as pressure-temperature phase stability, elastic properties and electrical conductivity (e.g. Roberge et al., 2015; Grützner et al., 2017b, 2018; Li et al., 2017; Ulian and Valdrè, 2017).

Dense hydrous magnesium silicates (DHMSs), important reservoirs for the distribution and transportation of water into the deep Earth (Litasov and Ohtani, 2003; Komabayashi and Omori, 2006), are also proposed to be hosts for F (Hazen et al., 1997). One of the DHMSs, superhydrous phase B (Shy—B) $Mg_{10}Si_3O_{18}H_4$ with 5.8 wt% H_2O, can be stable in the mantle transition zone (410–660 km) and even down to the uppermost lower mantle (e.g. Inoue et al., 2006; Litasov et al., 2007). It decomposes into phase D, bridgmanite and periclase at cold slab conditions or into bridgmanite, periclase and water in hot slabs at ~800 km depth (e.g. Ohtani et al., 2003). Elasticity and stability of Shy-B have been applied to explain geophysical observations, such as low shear velocity anomalies at the uppermost lower mantle and the discontinuity at ~800 km (Li et al., 2016; Yang et al., 2017). But little knowledge has been understood about the effects of both fluorine and hydrogen on the physicochemical properties of host minerals, limiting to further reveal the natural process of deep Earth. In this study, we synthesized two Shy-B samples, OH-rich $Mg_{9.86}Si_{3.14}O_{14}(F_{1.17},OH_{3.11})$ and F-rich $Mg_{9.96}Si_{3.04}O_{14}(F_{2.62},OH_{1.46})$ respectively. We conducted single-crystal X-ray diffraction (XRD) experiments up to ~27 GPa and 750 K, and then obtained their thermal equation of state. Based on the results, we discuss the influences of F on mantle minerals. It may have significant implications on the transportation of F from upper to lower mantle via subduction slabs and provides potential explanation for low-velocity zones at uppermost lower mantle.

2. Materials and methods

2.1. Samples synthesis and characterization

High-quality single-crystal OH-rich Shy-B and F-rich Shy-B labeled 5 K3408 were synthesized at 20 GPa and 1673 K for 7 h using USSA-5000 ton Kawai-type apparatus installed at Institute for Planetary Materials, Okayama University. The starting material of OH-rich Shy-B was a mixture of MgO, SiO_2, MgF_2, and $Mg(OH)_2$ with a molar ratio of 8:3:1:1. The starting material of F-rich Shy-B was a mixture of MgO, SiO_2 and MgF_2 with a molar ratio of 8:3:2. Two initial samples were placed together in an $Au_{80}Pd_{20}$ capsule of 2 mm in length and 2 mm in diameter, and then synthesized at the same condition. A Cr-doped MgO octahedron with an edge length of 14 mm was adopted as a pressure medium. Eight tungsten carbide anvils with a truncation of 6 mm were used as second-stage anvils. For the setup $LaCrO_3$ was used as a heater. The recovered samples are colorless single crystals with small grain size of ~200 μm for OH-rich Shy-B and ~ 100 μm for F-rich Shy-B, respectively. Sample characterization were performed at ambient conditions using scanning electron microscope (SEM) equipped with energy dispersive spectrometer (EDS) (Quanta 450 FEG), XRD (Rigaku XtaLAB PRO MM007HF), Raman spectroscopy (Horiba LabRAM HR Evolution) and electron microprobe analysis (EMPA). SEM and EDS results indicated that samples were chemically homogeneous with polyhedral shape (Fig. S1). The measurement conditions for F element were those used by Grützner et al. (2017a) and F concentrations in our two samples were determined with a synthetic multi-layered diffraction crystal (LDE). EMPA results show the composition of 61.78 wt% MgO, 29.34 wt % SiO_2, 3.46 wt% F and 60.68 wt% MgO, 27.66 wt% SiO_2, 7.53 wt% F for two samples, respectively, yielding the composition of $Mg_{9.86}Si_{3.14}O_{14}(F_{1.17},OH_{3.11})$ labeled OH-rich Shy-B and $Mg_{9.96}Si_{3.04}O_{14}(F_{2.62},OH_{1.46})$ labeled F-rich Shy-B. Their crystal structures are determined to be orthorhombic phase (*Pnnm* and Z = 2) with lattice constants of $a = 5.0826(2)$ Å, $b = 8.6772(3)$ Å, $c = 13.9911(5)$ Å, $V = 617.05(7)$ Å^3 for OH-rich Shy-B and $a = 5.0703(8)$ Å, $b = 8.6729(9)$ Å, $c = 13.8962(4)$ Å, $V = 611.07(11)$ Å^3 for F-rich Shy-B by a micro-focused X-ray diffractometer equipped with Mo *K*α radiation, respectively. Raman spectra of 16 grains picked randomly are in good agreement with those of Shy-B reported by Liu et al. (2002) (Fig. S2). The results of XRD, Raman spectroscopy, and EMPA demonstrate that the recovered products are pure phases without detectable impurities.

2.2. High-pressure synchrotron X-ray diffraction experiments

A short symmetry-type diamond anvil cell (DAC) equipped with Böhler-type diamond anvils of 300-μm flat culets anvils was employed to achieve high pressure and 60° opening for room temperature experiments. The sample chamber was formed by drilling a 190-μm-diameter hole in a rhenium gasket that had been pre-indented to ~38 μm in thickness. Two single-crystal samples of grain size ~40 × 40 × 15 μm^3 were together loaded into the sample chamber, as well as a piece of platinum for pressure calibration (Fei et al., 2007). Neon was employed as pressure transmitting medium using the COMPRES/GSECARS gas-loading system. In situ high-pressure single-crystal XRD experiments were carried out at beamline 13-BMC at Advanced Photon Source (APS), Argonne National Laboratory (ANL). A monochromatic X-ray beam with wavelength of 0.43409 Å was focused on a 15 × 15 μm^2 spot (Zhang et al., 2017). Wide-scan and stepped exposures were collected in a rotation range from −30° to 30° with 1° steps, with an exposure time of 1 s per frame. Diffraction images were reduced and analyzed using Bruker APEX3 software.

2.3. HTHP synchrotron radiation XRD experiments

In situ HTHP single-crystal XRD experiments were conducted up to 26.5 GPa with four different temperatures (300 K, 450 K, 600 K and 750 K) at beamline 13-BMC of APS. A BX90-type DAC equipped with 400-μm flat culets diamond anvils was used combined with an external heater. Two single-crystal samples polished on both sides and with a grain size of~30 × 30 × 15 μm^3 were loaded into sample chamber. They were prepared in the same way as the room temperature experiments. Platinum was employed as pressure maker and neon was used as pressure transmitting medium. A heater alumina ceramic was coiled by a single platinum wire of 200 μm diameter and ~45 cm in length. The measured resistance of heater was ~2 Ω. A K-type thermocouple attached close to sample chamber was used to determine temperatures. The GE PACE5000 membrane pressure controller was employed to remotely increase pressure. For each heating run the sample chamber was stabilized for at least 20 min at the given temperature to minimize temperature and pressure instability. X-ray diffraction images were collected and analyzed in the same way as the room temperature experiments.

3. Results and discussion

3.1. Equation of state

In situ high-pressure single-crystal XRD experiments were conducted up to ~27.8 GPa at room temperature. The refined unit-cell parameters of F-bearing Shy-B at various pressures have been listed in Table S1. The unit-cell volumes of both samples decrease monotonously with increasing pressure. The volumes as a function of pressure are plotted in Fig. 1, together with previous relevant data for comparison (Crichton

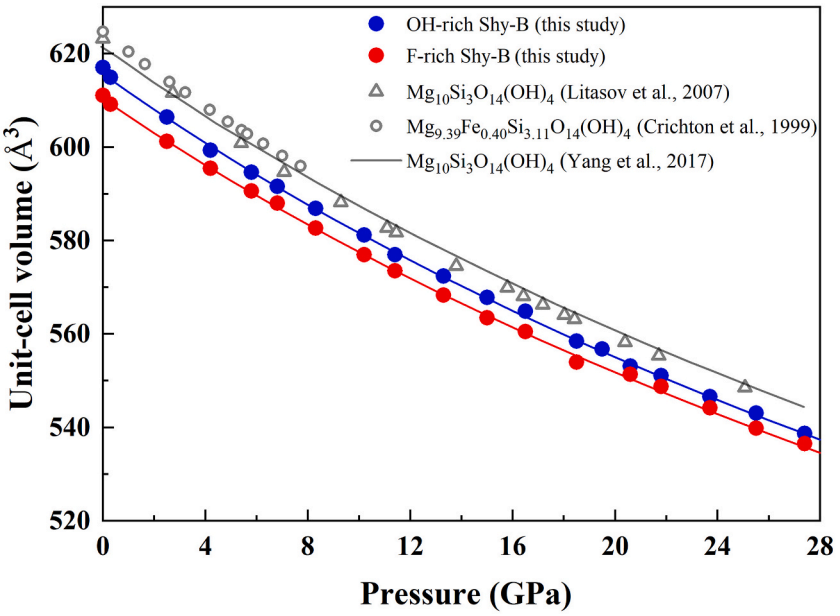

Fig. 1. Unit-cell volumes of F-bearing superhydrous phase B as a function of pressure up to 27.8 GPa. The solid blue and red circles represent OH-rich Shy-B and F-rich Shy—B, respectively. The solid blue and red curve are the fitting results by the second BM EoS based on the data of OH-rich and F-rich samples. The open gray circles and triangles represent the experimental data from Crichton et al. (1999) and Litasov et al. (2007). The solid gray line represents the results from literature data (Yang et al., 2017). Error bars are smaller than the symbol size for our data. (For interpretation of the references to color in this figure legend, the reader is referred to the web version of this article.)

et al., 1999; Litasov et al., 2007; Yang et al., 2017). The normalized stress ($F_E = P/[3f_E(2f_E+1)^{5/2}]$) as a function of the Eulerian finite strain ($f_E = [(V_0/V)^{2/3}-1]/2$) of Shy-B from our present experiments are plotted in Fig. 2. The slopes of the fitting results for Shy-B are almost flat, indicating that the second Birch-Murnaghan (BM) equation of state (EoS) is adequate. The pressure-volume data were fitted to the second order BM EoS with EoSFit7c (Angel et al., 2014). The fitting results are as follows: $V_0 = 615.6(2)$ Å^3, $K_0 = 156.9(9)$ GPa for the OH-rich sample, $V_0 = 610.3(1)$ Å^3, $K_0 = 162.0(6)$ GPa for F-rich Shy-B. The effects of F and water on the compressibility of Shy-B will be discussed in Section 3.3.

Fig. 3 shows the unit-cell volumes of two samples at high pressure and high temperature conditions and refined data were presented in Table S2. The experimental data were fitted by the second order BM thermal EoS (Test S1) up to 26.5 GPa and 750 K (Angel et al., 2014). The normalized stress F_E as a function of the Eulerian finite strain f_E of Shy-B at HTHP conditions from our present experiments are also plotted in Fig. 2. The slopes of the fitting results at different *P-T* conditions are in good agreement with that under room temperature. The thermoelastic parameters are as follows: $V_0 = 615.68(18)$, $K_0 = 158(7)$ GPa, $\partial K/\partial T =$ -0.020(4) GPa/K, $\alpha_0 = 4.5(2) \times 10^{-5}$ K^{-1} for OH-rich Shy-B and $V_0 =$ 610.38(7), $K_0 = 162(7)$ GPa, $\partial K/\partial T =$ -0.020(3) GPa/K, $\alpha_0 = 4.4(1) \times 10^{-5}$ K^{-1} for F-rich Shy-B. The thermal expansion coefficient of our two samples at atmospheric pressure are significantly larger than reported in previous studies for the OH end-member Shy-B with 3.8×10^{-5} K^{-1} by Inoue et al. (2006) and 3.2×10^{-5} K^{-1} by Litasov et al. (2007).

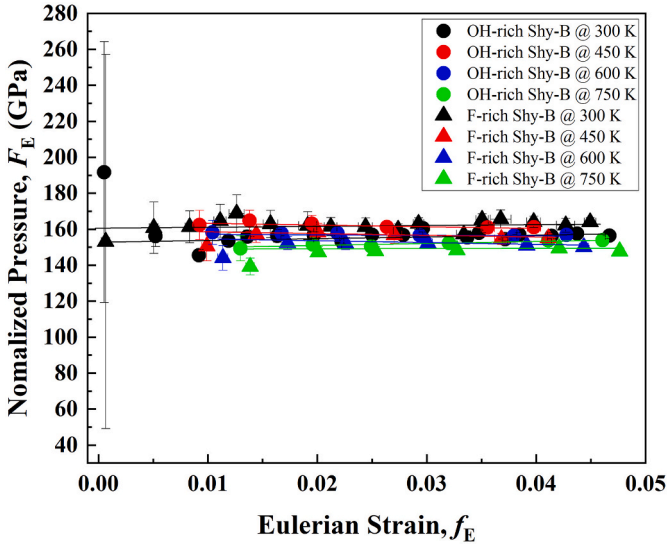

Fig. 2. Eulerian strain-normalized pressure (f_E-F_E) plot of unit cell volumes of F-bearing Shy-B at HTHP conditions from this study.

3.2. Axial compressibility of F-bearing Shy-B

To investigate the axial compressibility of F-bearing Shy-B, normalized unit-cell lattice parameters (a/a_0, b/b_0 and c/c_0) are plotted for comparison in Fig. S3 with respect to their ambient values for the two F-bearing Shy-B samples. No visible discontinuity has been observed in the axial compressibility of both samples up to 27.8 GPa. To determine the axial compressibility of *a*, *b*, and *c* of both samples, we used a linearized second order BM EoS fitting, where each axial dimension is cubed and treated as volume in BM formulation and the pressure derivatives are assumed to be 12. We fitted our linear moduli to a/a_0, b/b_0 and c/c_0 for OH-rich Shy-B are 448(18), 474(19), 477(7) GPa, while for F-rich Shy-B, we obtained linear moduli for a/a_0, b/b_0 and c/c_0 of 507(8), 510(20), and 459(18) GPa. There is no considerable anisotropy in axial compressibility in both samples, which in good agreement with previous results from Kudoh et al. (1994), Crichton et al. (1999), Shieh et al. (2000) and Litasov et al. (2007). It is obvious that the OH-rich Shy-B is more compressible than F-rich Shy-B for *a*- and *b*-axis. The results at high *P-T* conditions (Fig. S4) show that temperature has no effect on the axial compressional anisotropy.

3.3. Effects of F and water content on the density and compressibility of Shy-B

Shy-B with an ideal chemical formula of $Mg_{10}Si_3O_{14}(OH)_4$ containing 5.8 wt% water in its crystal structure. F can incorporate into Shy-B by replacing OH, like the case of humite minerals (e.g. Grützner et al., 2017b), indicating that the content of F and water in Shy-B show the negatively correlation with a formula of $Mg_{10}Si_3O_{14}(F_x,(OH)_{4-x})$. F has a smaller ionic radius and heavy atomic mass than those of OH, the substitution of OH by F would reduce the unit-cell volume and increase the density of minerals. Our results for F-bearing Shy-B show a smaller

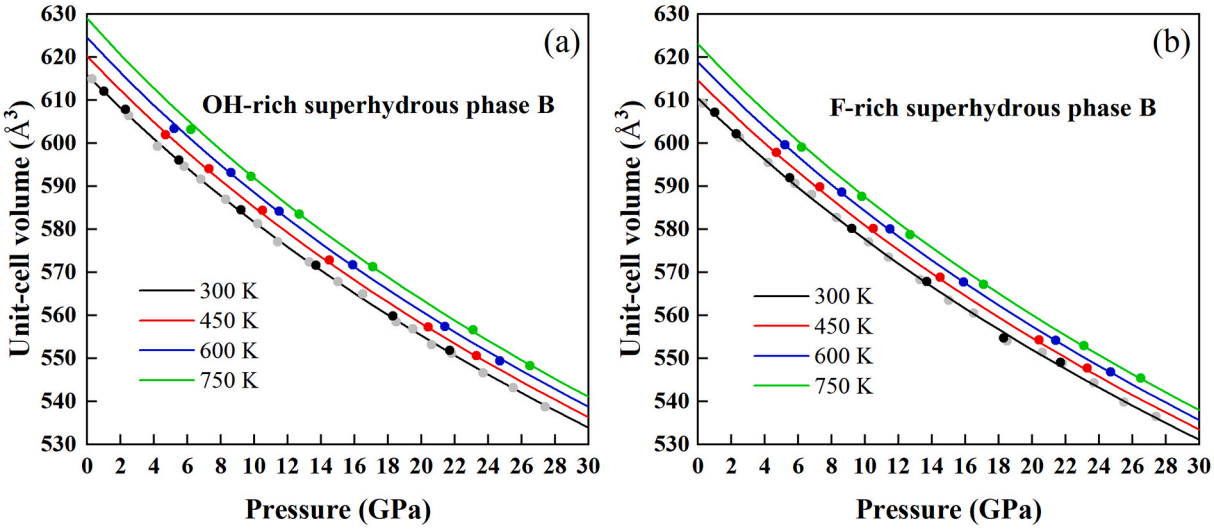

Fig. 3. *P-V-T* data obtained for (a) OH-rich Shy-B and (b) F-rich Shy-B in this study. The solid lines represent the isothermal compression curves from the high temperature 3rd-order B-M EoS at 300 K, 450 K, 600 K, and 750 K. The gray circles represent the high-pressure experimental data at room temperature in this study.

volume and larger density compared with those of OH-endmember (Fig. 4a and Table 1), supporting this view very well. Increasing water content presents an expansion effect on the unit-cell volume of olivine, wadsleyite and ringwoodite (Smyth and Jacobsen, 2006), but in the OH end-member Shy-B system it is no clearly tendency between water content and the unit-cell volume (Fig. 4a), which can be attributed to the large variations of Mg/Si ratio in Shy-B.

Due to the trade-off between K_0 and its pressure derivative (K_0'), we refitted the *P—V* data from literatures using the second-order BM EoS with a fixed $K_0' = 4$ for systematic comparison (Table 1). The K_0 of OH end-member Shy-B from XRD experiments in a range of 141.8–156.0 GPa. The Shy-B samples contain more or less water than ideal water content (5.8 wt%) attributed to the effect of some vacancies in the structure (Kudoh et al., 1994; Rosa et al., 2015; Li et al., 2016). Smyth and Jacobsen (2006) concluded that water has a softening effect on mantle minerals. The relationship between water content and K_0 of Shy-B have been plotted in Fig. 4b. Due to the large error bar from the data of Kudoh et al. (1994), it is hard to give a conclusion that the water content have an effect on the K_0 of OH end-member Shy-B (regardless of F-bearing Shy-B). Data also demonstrate that the K_0 of Shy-B is independent of the Mg/Si ratio (Table 1), which is consistent with that in phase D (Wu et al., 2016). We can find out that the K_0 of Shy-B increasing with decreasing water content if we take F-bearing Shy-B into account (Fig. 4b). As we mentioned above, F and OH occupy the same site in the structure of Shy-B and the solubility of F and OH in Shy-B show the negatively correlation. Thus, the statement of water softening Shy-B and F enhancing the incompressibility of Shy-B are the same. The unit-cell volume of F-rich Shy-B becomes closer to OH-rich Shy-B with increasing pressure (Fig. 1), which also demonstrate that F can enhance the incompressibility of Shy—B. To further explore the effect of F on the compressibility of Shy—B, we report the relationship between K_0 and K_0' (Fig. S5a). K_0 and K_0' of Shy-B range significantly, from 136 to 166 GPa for K_0 and from 3 to 5.8 for K_0'. The presence of F in Shy-B presents a trend of increasing K_0 and decreasing K_0'. The great influence of F on the compressibility have also been reported by previous studies. For example, humite minerals are important represents for the OH and F substitute for each other. F-bearing chondrodite, a humite mineral, has a higher bulk modulus than that of synthetic OH-chondrodite (Kuribayashi et al., 1998; Ross and Crichton, 2001 and references therein), also indicating that F enhance the incompressibility of minerals. Fig. S5b and Table S3 show plots of the bulk modulus against the density of DHMSs, which reveal a positive correlation between K_0 and density.

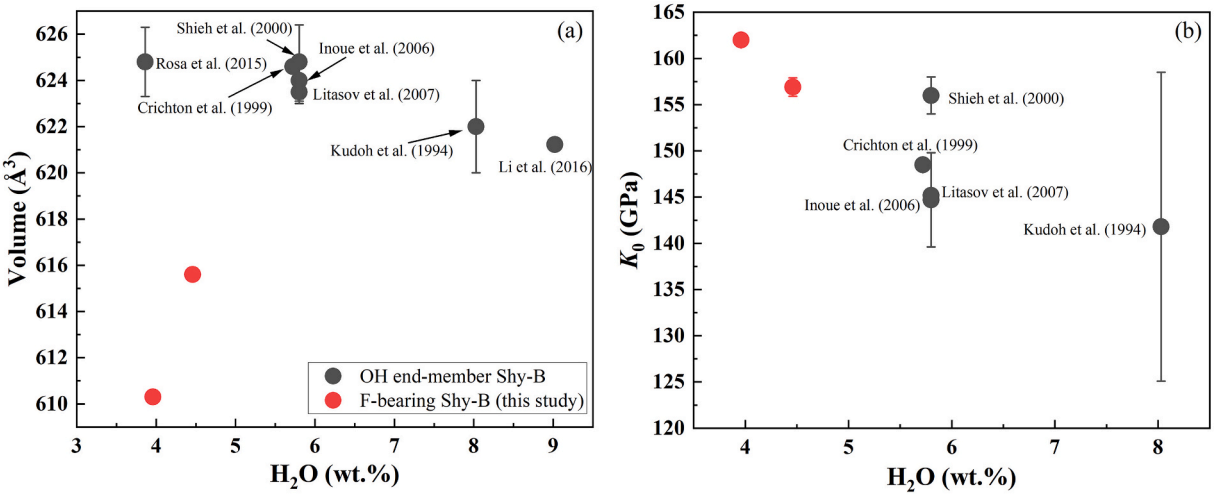

Fig. 4. (a) The relationship between water content and the volume of Shy—B. (b) Plot of bulk modulus (K_0) versus water content for Shy—B. Data were listed in Table 1.

Table 1
Isothermal bulk moduli K_T and density (ρ) of Shy—B. The K_T from XRD experiments have been refitted by the second order BM EoS.

Formula	V_0 (Å^3)	ρ (g/cm^3)	K_T (GPa)	K_0'	T (K)	Methed	References
$Mg_{9.86}Si_{3.14}O_{14}(F_{1.17},OH_{3.11})$	615.6(2)	3.381(2)	156.9(9)	4.0 (fixed)	300	DAC, single-crystal XRD	This study OH-rich sample
$Mg_{9.96}Si_{3.04}O_{14}(F_{2.62},OH_{1.46})$	610.3(1)	3.406(3)	162.0(6)	4.0 (fixed)	300	DAC, single-crystal XRD	This study F-rich sample
$Mg_{9.68}Si_{2.96}O_{18}H_{4.83}$	622.0(20)	3.300(4)	141.8(167)	4.0 (fixed)	300	DAC, single-crystal XRD	Kudoh et al. (1994)
$Mg_{9.39}Fe_{0.4}Si_{3.11}O_{18}H_4$	624.6(0.7)	3.353(2)	148.5(6)	4.0 (fixed)	300	DAC, single-crystal XRD	Crichton et al. (1999)[a]
$Mg_{9.95}Fe_{0.05}Si_3O_{14}(OH)_4$	624.8(16)	3.300(20)	156.0(20)	4.0 (fixed)	300	DAC, powder XRD	Shieh et al. (2000)[a]
$Mg_{10}Si_3O_{14}(OH)_4$	624.2(16)	3.296(8)	144.7(51)	4.0 (fixed)	300	MAA, powder XRD	Inoue et al. (2006)
$Mg_{9.98}Si_{3.01}O_{14}(OH)_4$	623.5(4)	3.300(10)	145.2(0.4)	4.0 (fixed)	300	MAA, powder XRD	Litasov et al. (2007)
$Mg_{10.4}Si_{3.1}O_{18}H_{2.7}$	624.8(15)	3.339(4)	147.3(1.5)	4.7(2)	300	DAC, Brillouin	Rosa et al. (2015)
$Mg_{9.38}Si_{2.81}H_{6.01}O_{18}$	621.23	3.197(5)	140.3(9)	4.0(1)	300	DAC, Brillouin	Li et al. (2016)
$Mg_{10}Si_3O_{14}(OH)_4$	618.2	3.327	154.0	4.3	Static	First principles calculation	Poswal et al. (2010)[b]
$Mg_{10}Si_3O_{14}(OH)_4$	598.5	3.437	161.8(0.2)	4.4(0.1)	Static	First principles calculation	Mookherjee and Tsuchiya, 2015[b]
$Mg_{10}Si_3O_{14}(OH)_4$	621.494	3.310	159.23	4	300	First principles calculation	Yang et al. (2017)[b]

Abbreviations: MAA, Multi-Anvil apparatus; XRD, X-ray diffraction; DAC, diamond anvil cell.
[a] Fe-bearing samples.
[b] First-principles calculations.

4. Implications

4.1. Distributions of fluorine and water in the Earth's mantle

The knowledge of the amount and the distribution of H_2O and F in mantle minerals is extremely important because even a small amount of H_2O and F (several ppm level) can dramatically affect the physical and chemical properties of these minerals (e.g. deformation, electrical conduction and thermal stability) (Roberge et al., 2015; Grützner et al., 2017b, 2018; Li et al., 2017; Ulian and Valdrè, 2017). In the following, we discuss H_2O and F storage capacities in the Earth's mantle using the pyrolite model (Fig. 5) (Irifune and Ringwood, 1987). The water storage capacity at the bottom of the upper mantle can reach up to 0.15 wt% (Férot and Bolfan-Casanova, 2012). The mantle transition zone have the ability to comprise up to 1 wt% H_2O (Pearson et al., 2014). For the lower mantle, due to a negligible potential for H_2O incorporation in ferro-periclase (no more than 20 ppm water, Bolfan-Casanova et al., 2002) and the small volume ratio of Ca-perovskite (only 5 wt% of the lower mantle), we did not take them into account. Based on the latest data from Yoshino and Jaseem (2018) and Fu et al. (2019), the lower mantle can contain 0.075–0.47 wt% H_2O in the presence of Al and F. Using the solubility of F in mantle minerals (Roberge et al., 2015; Grützner et al., 2017a; Grützner et al., 2018; Yoshino and Jaseem, 2018), we find a storage potential of 3520 μg/g F for the upper mantle, 1266 μg/g F for the mantle transition zone and 9680 μg/g F for the uppermost lower mantle (neglecting the F content in ferro-periclase and Ca-perovskite like in the case of H_2O). Comparing both volatiles, we see a striking difference between the behavior of F and H_2O in the Earth's mantle (Fig. 5). Water is more likely to be stored in the mantle transition zone, but F is rather stored either above the transition zone or below. Therefore, the fractionation of water and F will occur during subduction, as water enters preferentially into the transition zone and F tends to remain in peridotite of the lowermost upper mantle. Also, F is likely to partition into bridgmanite rather than ringwoodite, depending on the significant contrast in solubility of F between Al-bearing bridgmanite and transition zone minerals at the 660 km seismic discontinuity.

DHMSs are important hosts to transport H_2O and F into the deep Earth (Hazen et al., 1997; Tsuchiya and Umemoto, 2019), due to their broad *P-T* stability (Ohtani et al., 2003; Wu et al., 2016) Shy-B and phase D both serve as transition zone-crossing carriers from the upper mantle down into the lower mantle. Several studies show that low F concentrations have a dramatic effect on the temperature stability of many hydrous minerals (Pamato et al., 2015; Walter et al., 2015; Grützner et al., 2017b). The OH endmember Shy-B can be stable up to 30 GPa and

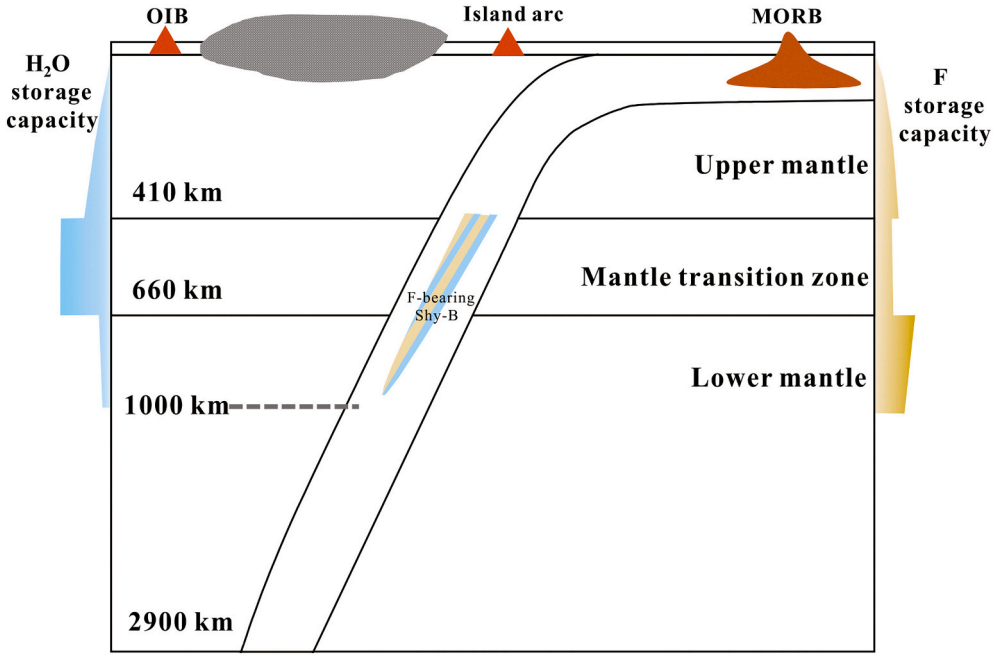

Fig. 5. Schematic model for global fluorine and water storage capacities. At left and right are schematic views of the H_2O and F storage capacity at different depth of Earth's mantle, respectively. We calculated the H_2O and F storage capacity in earth mantle using the pyrolite model (Irifune and Ringwood, 1987). Water storage capacity at the bottom of upper mantle can reach up to 0.15 wt% (Férot and Bolfan-Casanova, 2012). Mantle transition zone can comprise up to 1 wt% (Pearson et al., 2014), and the lower mantle can contain 0.075–0.47 wt% H_2O in presence of Al, Fe and F (Yoshino and Jaseem, 2018; Fu et al., 2019). F storage capacities have been calculated for the upper mantle (3520 μg/g). The mantle transition zone can store 741–1266 μg/g F and the uppermost lower mantle can store 9680 μg/g F. We see a striking difference the between behaviors of F and H_2O in Earth's mantle.

1673 K (Ohtani et al., 2003; Inoue et al., 2006; Litasov et al., 2007), while the fluorinated Shy-B approaches 1873 K (Gasparik and Drake, 1995). Thermal geodynamic modeling shows that some old and fast subducting slabs are only slowly heated on their way into the deeper mantle (Brown and Shankland, 1981). Hence, F-bearing Shy-B and Al-bearing phase D would be stable before the slab reaches ~1000 km (Brown and Shankland, 1981; Wu et al., 2016). So that partial melt formation by Shy-B and phase D breakdown in the uppermost lower mantle (660–800 km) is very unlikely. Instead, the downward flow of transition zone materials may be the primary contributor (Schmandt et al., 2014). F-bearing Shy-B break down into bridgmanite, periclase and water at ~1000 km (Komabayashi and Omori, 2006; Litasov and Ohtani, 2003). Then, F and H_2O may be incorporated into bridgmanite and form a small amount of (F, OH)-bearing bridgmanite in this region, since bridgmanite was reported to have the ability to incorporate larger amounts of F and H_2O (up to 10,000 ppm F and 4900 ppm H_2O, Yoshino and Jaseem, 2018; Fu et al., 2019).

4.2. Elasticity and influences of F-bearing Shy-B along subduction slabs

Recently, the seismic low velocity zone has been observed at depths of the uppermost lower mantle (Schmandt et al., 2014), which is attributed to the result of dehydration melting. Since Shy-B is a potential carrier of water to the uppermost lower mantle, the accumulation and decomposition of Shy-B has been employed to explain the observed low-velocity layers in this region (Li et al., 2016; Yang et al., 2017). To address the geophysical and geodynamic implications for a subducting slab, we have evaluated density (ρ) and bulk velocity (V_Φ) profiles of two samples as a function of pressure along cold and hot slab geotherms (Fig. 6). Mineral proportions in hydrous pyrolitic mantle are based on phase relations given by Litasov et al. (2007). Our modeled results show that the ρ of F-bearing Shy-B are lower than that of the preliminary reference Earth model (PREM) (Dziewonski and Anderson, 1981). This indicates that the presence of F-bearing Shy-B can contribute to a positive buoyancy force (Fig. 6). Previous study demonstrated that the presence of ~18 wt% OH end-member Shy-B at the uppermost lower mantle would reduce the density of the hydrated subducting slab by 1.9–2.1% (Inoue et al., 2006). Accordingly, a homogeneously hydrated and Fe-free slab may float at the bottom of the transition zone and would not be able to penetrate into the deep lower mantle (Inoue et al., 2006; Litasov et al., 2007). While, F-bearing Shy-B from this study are ~1.3–1.7% denser than OH end-member Shy-B for cold or hot slab geotherms. Shy-B may contain 10 wt% Fe in its structure, which can further enhance the density of Shy-B (Crichton et al., 1999; Litasov et al., 2007). If Shy-B contains 10 wt% Fe and 10 wt% F, the ρ of (Fe, F)-bearing Shy-B is 5% denser than the OH endmember along subduction slabs. The slab contains 18 wt% (Fe, F)-bearing Shy—B, the combined effect of Fe and F would enhance the ρ of slabs by ~0.8% compared with (Fe, F)-free hydrated slabs. As a result, the (Fe, F)-bearing slab have a similar ρ as the surrounding mantle rocks (Fig. 6).

Our results show that F-bearing Shy-B leads to an increase of ~1.8–2.4% in V_Φ relative to the OH end-member at cold slab geotherms. Meanwhile, it increases by ~1.0–2.1% at hot slab geotherms. Li et al. (2016) reported that ~17–26 wt% Fe-free Shy-B in the peridotite layer could help explain the velocity anomalies at the uppermost lower mantle. However, the difference in the bulk sound velocity between F-bearing Shy-B and PREM is ~0.3–2% in cold and hot slabs at the topmost lower mantle, indicating that we need more amount of Shy-B than previous predicted (Li et al., 2016). Therefore, it is difficult to explain the velocity anomalies using such simple model, especially in fluorine rich slabs. So far, we have no data for the velocity of Fe-bearing Shy—B. But iron component generally makes silicates becoming soften and denser because of larger cation radius and higher atomic weight, reducing the hosts' velocities significantly (e.g. bridgmanite and post-perovskite, Tsuchiya and Tsuchiya, 2006). Therefore, (Fe, F)-bearing Shy-B might be a potential source of the low velocity anomalies at the

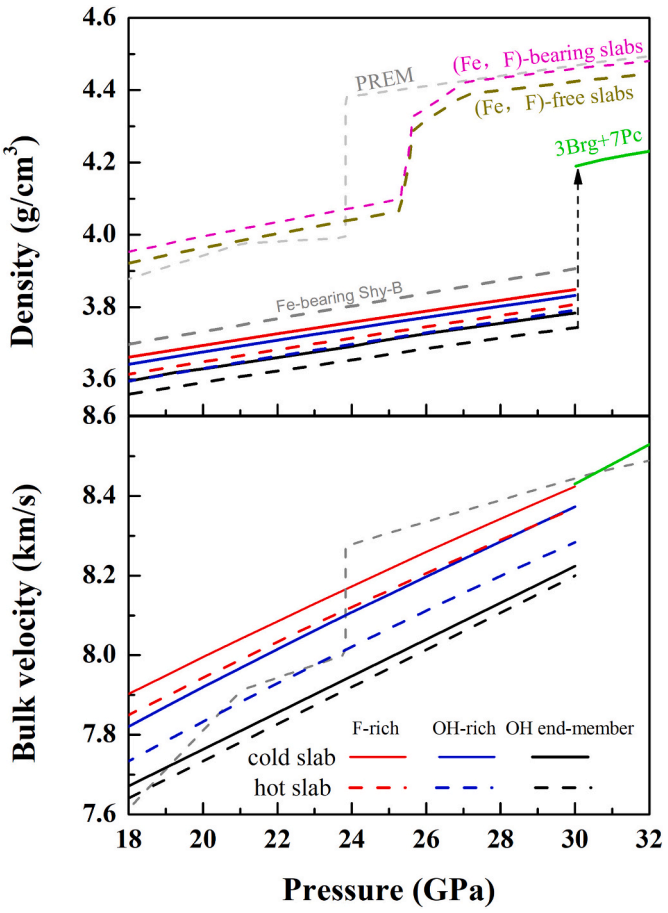

Fig. 6. Density (ρ) and bulk sound velocity (V_Φ) of the two samples compared with the preliminary reference Earth model (PREM) (Dziewonski and Anderson, 1981) and the aggregate of 7 iron-free bridgmanite (Brg) + 3 periclase (Pc) under both cold (900 K) and hot (1300*K*) slabs geotherms. The density for subduction slabs contain ~18% (Fe, F)-bearing Shy-B (dash line with magenta color) and for subduction slabs contain ~18% (Fe, F)-free Shy-B (dash line with dark yellow color) (Litasov et al., 2007) are plotted for comparison. (For interpretation of the references to color in this figure legend, the reader is referred to the web version of this article.)

uppermost lower mantle. Here, we also modeled changes of V_Φ across these phases transition (Fig. 6) and we calculated V_Φ for 3 bridgmanite and 7 periclase assembly combined with their elasticities from Yang et al. (2017). As there are currently no parameters available for F-bearing bridgmanite and periclase, we use the data of (F, H_2O)-free bridgmanite ($MgSiO_3$) and periclase (Yang et al., 2017) as the best approximation. Our results show that only a small V_Φ increase of ~1.8% and ~ 0.7% along hot subducted slabs. In cold subducted slabs, the V_Φ of F-bearing Shy-B is almost consistent with the breakdown products. Although the effect of Fe on the V_Φ of phase transition from Shy-B to bridgmanite and periclase has not been investigated in this study, we believe that Fe in Shy-B should not change significantly these values since Fe shows an approximate influence on velocities in several mantle minerals (e.g. 1% Fe reduces the shear velocity of periclase and bridgmanite by ~0.03 km/s at ambient conditions; Muir and Brodholt, 2015; Shukla et al., 2015).

Author contributions

Xiang Li: Designed research, Performed research, Analyzed data.
Yungui Liu: Designed research, Performed research, Analyzed data.
Ran Wang: Performed research.
Takashi Yoshino: Designed research, Performed research.

Jingui Xu: Performed research.
Dongzhou Zhang: Performed research.
Tobias Grützner: Designed research.
Junfeng Zhang: Designed research.
Xiang Wu: Designed research, Performed research, Analyzed data.
All authors participated in writing the paper.

Declaration of Competing Interest

The authors declare that they have no known competing financial interests or personal relationships that could have appeared to influence the work reported in this paper.

Acknowledgments

X. Wu acknowledges financial support from the National Science Foundation of China (41473056 and 41827802). We also thank Dr. Kei Hirose and two anonymous reviewers for their constructive comments to improve the quality of the article. This work is supported by a joint research program at the Institute for Planetary Materials, Okayama University. We would like to thank Sergey Tkachev for gas loading the diamond anvil cells, Qian Zhang and Haipeng Song for experiment preparations. This work was performed at GeoSoilEnviroCARS, Advanced Photon Source (APS), Argonne National Laboratory (ANL). GeoSoilEnviroCARS operations are supported by the National Science Foundation-Earth Sciences (EAR-1634415) and the Department of Energy, Geosciences (DE-FG02-94ER14466). APS is supported by DOE-BES, under Contract No. DE-AC02-06CH11357. PX2 and the GSECARS/COMPRES gas loading system are supported in part by COMPRES under NSF Cooperative Agreement EAR-1661511. All the data to produce all the figures in this paper are available on Zenodo (doi: https://doi.org/10.5281/zenodo.3993846).

Appendix A. Supplementary data

Supplementary data to this article can be found online at https://doi.org/10.1016/j.pepi.2021.106824.

References

Angel, R.J., Alvaro, M., Gonzalez-Platas, J., 2014. EosFit7c and a Fortran module (library) for equation of state calculations. Zeitschrift für Kristallographie Crystal. Mater. 229, 405–419. https://doi.org/10.1515/zkri-2013-1711.

Bernini, D., Wiedenbeck, M., Dolejš, D., Keppler, H., 2012. Partitioning of halogens between mantle minerals and aqueous fluids: implications for the fluid flow regime in subduction zones. Contrib. Mineral. Petrol. 165, 117–128. https://doi.org/10.1007/s00410-012-0799-4.

Bolfan-Casanova, N., Mackwell, S., Keppler, H., McCammon, C., Rubie, D.C., 2002. Pressure dependence of H solubility in magnesiowüstite up to 25 GPa: implications for the storage of water in the Earth's lower mantle. Geophys. Res. Lett. *29* https://doi.org/10.1029/2001GL014457, 81-1-81-4.

Brown, J.M., Shankland, T.J., 1981. Thermodynamic parameters in the Earth as determined from seismic profiles. Geophys. J. R. Astron. Soc. 66, 579–596. https://doi.org/10.1111/j.1365-246X.1981.tb04891.x.

Crichton, W.A., Ross, N.L., Gasparik, T., 1999. Equations of state of magnesium silicates anhydrous B and superhydrous B. Phys. Chem. Miner. 26, 570–575. https://doi.org/10.1007/s002690050220.

Dalou, C., Koga, K.T., Shimizu, N., Boulon, J., Devidal, J.-L., 2012. Experimental determination of F and Cl partitioning between lherzolite and basaltic melt. Contrib. Mineral. Petrol. 163, 591–609. https://doi.org/10.1007/s00410-011-0688-2.

Dziewonski, A.M., Anderson, D.L., 1981. Preliminary reference Earth model. Phys. Earth Planet. Inter. 25, 297–356. https://doi.org/10.1016/0031-9201(81)90046-7.

Fei, Y., Ricolleau, A., Frank, M., Mibe, K., Shen, G., Prakapenka, V., 2007. Toward an internally consistent pressure scale. Proc. Natl. Acad. Sci. *104*, 9182–9186. https://doi.org/10.1073/pnas.0609013104.

Férot, A., Bolfan-Casanova, N., 2012. Water storage capacity in olivine and pyroxene to 14 GPa: implications for the water content of the Earth's upper mantle and nature of seismic discontinuities. Earth Planet. Sci. Lett. 394, 218–230. https://doi.org/10.1016/j.epsl.2012.06.022.

Fu, S.Y., Yang, J., Karato, S.-I., Vasiliev, A., Presniakov, M.Y., Gavrilliuk, A.G., et al., 2019. Water concentration in single-crystal (Al,Fe)-bearing bridgmanite grown from the hydrous melt: implications for dehydration melting at the topmost lower mantle. Geophys. Res. Lett. 46, 10346–10357. https://doi.org/10.1029/2019GL084630.

Gasparik, T., Drake, M.J., 1995. Partitioning of elements among two silicate perovskites, superphase B, and volatile-bearing melt at 23 GPa and 1500-1600°C. Earth Planet. Sci. Lett. 134, 307–318. https://doi.org/10.1016/0012-821X(95)00133-W.

Grützner, T., Kohn, S.C., Bromiley, D.W., Rohrbach, A., Berndt, J., Klemme, S., 2017a. The storage capacity of fluorine in olivine and pyroxene under upper mantle conditions. Geochim. Cosmochim. Acta 208, 160–170. https://doi.org/10.1016/j.gca.2017.03.043.

Grützner, T., Klemme, S., Rohrbach, A., Gervasoni, F., Berndt, J., 2017b. The role of F-clinohumite in volatile recycling processes in subduction zones. Geology 45, 443–446. https://doi.org/10.1130/G38788.1.

Grützner, T., Klemme, S., Rohrbach, A., Gervasoni, F., Berndt, J., 2018. The effect of fluorine on the stability of wadsleyite: implications for the nature and depths of the transition zone in the Earth's mantle. Earth Planet. Sci. Lett. 482, 236–244. https://doi.org/10.1016/j.epsl.2017.11.011.

Hazen, M., Yang, H., Prewitt, C.T., Gasparik, T., 1997. Crystal chemistry of superfluorous phase B ($Mg_{10}Si_3O_{14}F_4$): implications for the role of fluorine in the mantle. Am. Mineral. 82, 647–650. https://doi.org/10.2138/am-1997-5-626.

Inoue, T., 1994. Effect of water on melting phase relations and melt composition in the system Mg_2SiO_4–$MgSiO_3$–H_2O up to 15 GPa. Phys. Earth Planet. Inter. 85, 237–263. https://doi.org/10.1016/0031-9201(94)90116-3.

Inoue, T., Ueda, T., Higo, Y., Yamada, A., Irifune, T., Funakoshi, K.I., 2006. High-pressure and high-temperature stability and equation of state of superhydrous phase B. In: Jacobsen, S.D., Lee, S. (Eds.), Earth's Deep Water Cycle. AGU, Washington, D. C, pp. 147–157.

Irifune, T., Ringwood, A.E., 1987. Phase transformations in a harzburgite composition to 26 GPa: implications for dynamical behaviour of the subducting slab. Earth Planet. Sci. Lett. 86, 365–376. https://doi.org/10.1016/0012-821X(87)90233-0.

Joachim, B., Pawley, A., Lyon, I.C., Marquardt, K., Henkel, T., Clay, P.L., et al., 2015. Experimental partitioning of F and Cl between olivine, orthopyroxene and silicate melts at Earth's mantle conditions. Chem. Geol. 416, 65–78. https://doi.org/10.1016/j.chemgeo.2015.08.012.

John, T., Scambelluri, M., Frische, M., Barnes, J.D., Bach, W., 2011. Dehydration of subducting serpentinite: implications for halogen mobility in subduction zones and the deep halogen cycle. Earth Planet. Sci. Lett. 308, 65–76. https://doi.org/10.1016/j.epsl.2011.05.038.

Kohlstedt, D., Keppler, H., Rubie, D.C., 1996. Solubility of water in the α, β and γ phases of $(Mg,Fe)_2SiO_4$. Contrib. Mineral. Petrol. 123, 345–357. https://doi.org/10.1007/s004100050161.

Komabayashi, T., Omori, S., 2006. Internally consistent thermodynamic data set for dense hydrous magnesium silicates up to 35GPa, 1600°C: implications for water circulation in the Earth's deep mantle. Phys. Earth Planet. Inter. 156, 89–107. https://doi.org/10.1016/j.pepi.2006.02.002.

Kudoh, Y., Nagase, T., Ohta, S., Sasaki, S., Kanzaki, M., Tanaka, M., 1994. Crystal-structure and compressibility of superhydrous phase-B, $Mg_{20}Si_6H_8O_{36}$, paper presented at AIP Conf. In: Proc., Colorado Springs, Colo.

Kuribayashi, T., Kudoh, Y., Akizuki, M., 1998. Single-crystal X-ray diffraction and FTIR spectra of chondrodite, $Mg_5Si_2O_8(OH,F)_2$ under high pressure to 6.0 GPa. In: 17th General Meeting of the International Mineralogical Association, Toronto, A44.

Li, X.Y., Mao, Z., Sun, N.Y., Liao, Y.F., Zhai, S.M., Wang, Y., et al., 2016. Elasticity of single-crystal superhydrous phase B at simultaneous high pressure-temperature conditions. Geophys. Res. Lett. 43, 8458–8465. https://doi.org/10.1002/2016GL070027.

Li, Y., Jiang, H., Yang, X., 2017. Fluorine follows water: effect on electrical conductivity of silicate minerals by experimental constraints from phlogopite. Geochim. Cosmochim. Acta 217, 16–27. https://doi.org/10.1016/j.gca.2017.08.020.

Litasov, K.D., Ohtani, E., 2003. Stability of hydrous phases in CMAS pyrolite-H_2O system up to 25 GPa. Phys. Chem. Miner. 30, 147–156. https://doi.org/10.1007/s00269-003-0301-y.

Litasov, K.D., Ohtani, E., Ghosh, S., Nishihara, Y., Suzuki, A., Funakoshi, K., 2007. Thermal equation of state of superhydrous phase B to 27 GPa and 1373 K. Phys. Earth Planet. Inter. 164, 142–160. https://doi.org/10.1016/j.pepi.2007.06.003.

Liu, L.G., Lin, C.C., Mernagh, T.P., Inoue, T., 2002. Raman spectra of phase C (superhydrous phase B) at various pressures and temperatures. Eur. J. Mineral. 15, 15–23. https://doi.org/10.1127/0935-1221/2002/0014-0015.

McDonough, W.F., Sun, S.-S., 1995. The composition of the Earth. Chem. Geol. 120, 223–253. https://doi.org/10.1016/0009-2541(94)00140-4.

Mookherjee, M., Tsuchiya, J., 2015. Elasticity of superhydrous phase, B, $Mg_{10}Si_3O_{14}(OH)_4$. Phys. Earth Planet. Inter. 238, 42–50. https://doi.org/10.1016/j.pepi.2014.10.010.

Mosenfelder, J.L., Rossman, G.R., 2013a. Analysis of hydrogen and fluorine in pyroxenes: I. Orthopyroxene. Am. Mineral. 98, 1026–1041. https://doi.org/10.2138/am.2013.4291.

Mosenfelder, J.L., Rossman, G.R., 2013b. Analysis of hydrogen and fluorine in pyroxenes: II. Clinopyroxene. Am. Mineral. 98, 1042–1054. https://doi.org/10.2138/am.2013.4413.

Muir, J.M.R., Brodholt, J.P., 2015. Elastic properties of ferropericlase at lower mantle conditions and its relevance to ULVZs. Earth Planet. Sci. Lett. 417, 40–48. https://doi.org/10.1016/j.epsl.2015.02.023.

Ohtani, E., Toma, M., Kubo, T., Kondo, T., Kikegawa, T., 2003. In situ X-ray observation of decomposition of superhydrous phase B at high pressure and temperature. Geophys. Res. Lett. 30, 1029. https://doi.org/10.1029/2002GL015549.

Pamato, M.G., Muhill, R., Ballaran, T.B., Frost, D.J., Heidelbach, F., Miyajima, N., 2015. Lower-mantle water reservoir implied by the extreme stability of a hydrous aluminosilicate. Nat. Geosci. 8, 75–79. https://doi.org/10.1038/NGEO2306.

Pearson, D.G., Brenker, F.E., Nestola, F., McNeill, J., Nasdala, L., Hutchison, M.T., et al., 2014. Hydrous mantle transition zone indicated by ringwoodite included within diamond. Nature 507, 221–224. https://doi.org/10.1038/nature13080.

Poswal, H.K., Sharma, S.M., Sikka, S.K., 2010. Investigation of structure and hydrogen bonding of superhydrous phase B (HT) under pressure using first-principles density functional calculations. High Pressure Res. 30, 198–206. https://doi.org/10.1080/08957950903503920.

Roberge, M., Bureau, H., Bolfan-Casanova, N., Frost, D.J., Raepsaet, C., Surble, S., et al., 2015. Is the transition zone a deep reservoir for fluorine? Earth Planet. Sci. Lett. 429, 25–32. https://doi.org/10.1016/j.epsl.2015.07.051.

Rosa, A.D., Sanchez-Valle, C., Wang, J.Y., Saikia, A., 2015. Elasticity of superhydrous phase B, seismic anomalies in cold slabs and implications for deep water transport. Phys. Earth Planet. Inter. 243, 30–43. https://doi.org/10.1016/j.pepi.2015.03.009.

Ross, N.L., Crichton, W.A., 2001. Compression of synthetic hydroxylclinohumite [$Mg_9Si_4O_{16}(OH)_2$] and hydroxylchondrodite [$Mg_5Si_2O_8(OH)_2$]. Am. Mineral. 86, 990–996. https://doi.org/10.2138/am-2001-8-905.

Saal, A.E., Hauri, E.H., Langmuir, C.H., Perfit, M.R., 2002. Vapour undersaturation in primitive mid-ocean-ridge basalt and the volatile content of Earth's upper mantle. Nature 419, 451–455. https://doi.org/10.1038/nature01073.

Schilling, J.-G., Bergeron, M.B., Evans, R., 1980. Halogens in the mantle beneath the North Atlantic. Philos. Trans. 297, 147–178.

Schmandt, B., Jacobsen, S.D., Becker, T.W., Liu, Z., Dueker, K.G., 2014. Dehydration melting at the top of the lower mantle. Science 344, 1265–1268. https://doi.org/10.1126/science.1253358.

Shieh, S.R., Mao, H.K., Hemley, R.J., Ming, L.C., 2000. In situ X-ray diffraction studies of dense hydrous magnesium silicates at mantle conditions. Earth Planet. Sci. Lett. 177, 69–80. https://doi.org/10.1016/S0012-821X(00)00033-9.

Shukla, G., Wu, Z.Q., Hsu, H., Floris, A., Cococcioni, M., Wentzcovitch, R.M., 2015. Thermoelasticity of Fe^{2+}-bearing bridgmanite. Geophys. Res. Lett. 42, 1741–1749. https://doi.org/10.1002/2014GL062888.

Smyth, J.R., 1987. β-Mg_2SiO_4: a potential host for water in the mantle? Am. Mineral. 72, 1051–1055.

Smyth, J.R., Jacobsen, S.D., 2006. Nominally Anhydrous Minerals and Earth's Deep Water Cycle. Earth's Deep Water Cycle, Geophysical Monograph Series, pp. 1–11. https://doi.org/10.1029/168gm02.

Straub, S.M., Layne, G.D., 2003. The systematics of chlorine, fluorine, and water in Izu arc front volcanic rocks: implications for volatile recycling in subduction zones. Geochim. Cosmochim. Acta 67, 4179–4203. https://doi.org/10.1016/S0016-7037(03)00307-7.

Tsuchiya, T., Tsuchiya, J., 2006. Effect of impurity on the elasticity of perovskite and postperovskite: velocity contrast across the postperovskite transition in (Mg,Fe,Al)(Si,Al)O_3. Geophys. Res. Lett. 33, 1–4. https://doi.org/10.1029/2006GL025706.

Tsuchiya, J., Umemoto, K., 2019. First-principles determination of the dissociation phase boundary of phase H $MgSiO_4H_2$. Geophys. Res. Lett. 46, 7333–7336. https://doi.org/10.1029/2019gl083472.

Ulian, G., Valdrè, G., 2017. Effects of fluorine content on the elastic behavior of topaz [$Al_2SiO_4(F,OH)_2$]. Am. Mineral. 102, 347–356. https://doi.org/10.2138/am-2017-5668.

Walter, M.J., Thomson, A.R., Wang, W., Lord, O.T., Ross, J., McMahon, S.C., et al., 2015. The stability of hydrous silicates in Earth's lower mantle: experimental constraints from the systems MgO–SiO_2–H_2O and MgO–Al_2O_3–SiO_2–H_2O. Chem. Geol. 418, 16–29. https://doi.org/10.1016/j.chemgeo.2015.05.001.

Wu, X., Wu, Y., Lin, J.F., Liu, J., Mao, Z., Guo, X., et al., 2016. Two-stage spin transition of iron in Fe,Al-bearing phase D at lower mantle. J. Geophys. Res. 121, 6411–6420. https://doi.org/10.1002/2016JB013209.

Yang, D., Wang, W.Z., Wu, Z.Q., 2017. Elasticity of superhydrous phase B at the mantle temperatures and pressures: implications for 800 km discontinuity and water flow into the lower mantle. J. Geophys. Res. 122, 5026–5037. https://doi.org/10.1002/2017JB014319.

Yoshino, T., Jaseem, V., 2018. Solubility in bridgmanite: a potential fluorine reservoir in the Earth's mantle. Earth Planet. Sci. Lett. 504, 106–114. https://doi.org/10.1016/j.epsl.2018.10.009.

Zhang, D.Z., Dera, P., Eng, P.J., Stubbs, J.E., Zhang, J.S., Prakapenka, V.B., et al., 2017. High pressure single crystal diffraction at PXˆ2. Jove 119, e54660. https://doi.org/10.3791/54660.